

and *Naringi crenulata*, which represent 53.94% of the total importance value index (IVI) (Table 1). The third species based on IVI value was *Tectona grandis*, which contributes only 6% of total IVI. The population includes a total of 20 species in which 13 were poorly represented with less than 2% in relative IVI. In addition, sandal excels all other species in phytosociological data with 31% of IVI, more than 36% of total basal area, more than 38% of total density (390 individuals/ha); it is the only species with 100% frequency of distribution in the study area (Table 1). This indicates that the edaphic and climatic factors in the study area are highly suitable for *S. album* and hence provides an opportunity for thorough exploration in adjacent areas for new sandal populations. Detailed studies are also required to understand the regeneration pattern, population dynamics and total number of sandal trees in the entire population. Phenotypic characterization, genetic diversity assessment and wood characterization for comparing with other populations are also suggested for developing tree improvement and *ex situ* conservation programmes. Based on our observations, the existing staff pattern of the Forest Department is to be revised for ensuring proper protection of the described sandal population. Officials of the Forest Department are making efforts to conserve the population with their limited human resource. A detailed study on this population with the following objectives is suggested to develop strategies for conservation and sustainable utilization

of sandalwood resources of this particular population:

- Generate baseline information on total number of trees in different girth classes and up-to-date assessment of sandalwood volume.
- Assess the quality of heartwood.
- Analyse the regeneration pattern and population dynamics to understand and assess the threats to the population.
- Determine genetic structure of the population, especially genetic variability within and between populations, and significant level of gene flow between and among populations.
- Assess current conservation and management activities to develop improved strategies.

1. Srinivasan, V. V., Sivaramakrishnan, V. R., Rangaswamy, C. R., Ananthapadmanabha, H. S. and Shankaranarayana, K. H., *Sandal (Santalum album L.)*, ICFRE, Dehra Dun, 1992.
2. Jain, S. H., Angadi, V. G., Rajeevalochan, A. N., Shankaranarayana, K. H., Theagarajan, K. S. and Rangaswamy, C. R., In *Sandal and its Products* (eds Radomiljac, A. M. et al.), Australian Centre for International Agricultural Research (ACIAR) Proceedings (84), Canberra, Australia, 1998, pp. 117–120.
3. Srimathi, R. A., Kulkarni, H. D. and Venkatesan, K. R., In *Recent Advances in Research and Management of Santalum album L. in India* (eds Srimathi, R. A. et al.), Associated Publishing Co, New Delhi, 1995, p. 416.

4. Suma, T. B. and Balasundaran, M., *Indian J. Genet.*, 2004, **64**(1), 13–16.
5. Parthiban, K. T., Surendran, C., Muruges, M. and Bhuvaneshwaran, C., In *Sandal and its Products* (eds Radomiljac, A. M.), ACIAR Proceedings. No. 84, ACIAR, Canberra, Australia, 1998, p. 7478.
6. Jeeva, V., Saravanan, S., Devaraj, P. and Lakshmidivi, R., In *Sandal and its Products* (eds Radomiljac, A. M. et al.), ACIAR Proceedings, No. 84, ACIAR, Canberra, Australia, 1998, p. 16.
7. Rao, M. N., Ganeshiah, K. N. and Uma Shaanker, R., *Conserv. Genet.*, 2007, **8**, 925–935; ISSN 1566-0621.
8. Swaminathan, M. H., Hosmath, B. J. and Mallesha, B. B., In *Sandal and its Products* (eds Radomiljac, A. M. et al.), ACIAR Proceedings (84), IWST & KSFD, Bengaluru, 1998, pp. 3–5.

ACKNOWLEDGEMENTS. We thank Director, Kerala Forest Research Institute, Peechi for support and encouragement. We also thank the Divisional Forest Officer, Mannarkad and Range Officer, Agali and other officials of Kerala Forest Department for their support during field work.

Received 16 March 2015; revised accepted 3 September 2015

K. A. SREEJITH\*  
V. B. SREEKUMAR  
T. K. NIRMESH  
R. SUGANTHASAKTHIVEL

*Forest Ecology and Biodiversity  
Conservation Division,  
Kerala Forest Research Institute,  
Peechi 680 653, India  
\*For correspondence  
e-mail: sreejith@kfri.res.in*

## Thermal anomaly from NOAA data for the Nepal earthquake

The Himalaya originated as a result of the collision of the northward-moving Indian continent with the Eurasian continent. Due to the continued impingement of the Indian plate, sufficient strain got accumulated, and the recent earthquake of 25 April 2015 took place in near Kathmandu, Nepal (epicenter 28.3°N, 84.5°E with magnitude 7.8 on the Richter scale and focal depth approximately 8 km)<sup>1,2</sup> due to thrust faulting. The study area comprises a large part of central and far-western Nepal (Figure 1) for monitor-

ing the thermal anomalies associated with this earthquake. The tectonic features in Figure 1 have been taken from GSI<sup>3</sup>.

Nepal is located in the central sector of the southwardly convex Himalayan mountain arc. Nepal Himalaya, occupying the central 800 km part, can be divided into five distinct geotectonic zones from south to north as follows: (1) Terai Plain, (2) Sub-Himalaya (Siwalik Range), (3) Lesser Himalaya, (4) Higher Himalaya and (5) Inner Himalaya (Tibetan Tethys).

Each of these zones can be identified by its distinct tectonic, morphologic and geologic features<sup>4</sup>. The main seismotectonic boundaries characterized as thrusts from south to north are the Main Frontal Thrust (MFT), Main Boundary Thrust (MBT) and Main Central Thrust (MCT), which are the boundary lines between the two consecutive units of Lesser Himalaya and Higher Himalaya<sup>5</sup>. Figure 2 presents a schematic representation of these features with respect to the Himalayan topography, basement slab and Himalayan

Frontal Thrust (HFT)/MFT in the foothills<sup>6</sup>.

Tectonic activities that cause earthquakes are largely associated with pressure build-up and subsurface degassing<sup>7</sup>, which in turn results in certain changes in the thermal regime. This is termed as ‘thermal anomaly’. Major part of the convergence between India and Tibet is transformed into elastic strain energy<sup>1</sup>. The increased strain conditions may have caused subsurface groundwater changes and release of different gases like CO<sub>2</sub>, CH<sub>4</sub> and N<sub>2</sub> to the lower atmosphere, which enhances the local greenhouse effect. This in turn may result in certain changes in the thermal regime causing a heating effect that leads to the appearance of a thermal anomaly. The Nepal earthquake occurred on the MHT and

must have had an impact on the MFT (frontal Himalayan region) too<sup>5</sup>. Since rock formations in the Siwalik region are more porous and permeable than the Lesser and Higher Himalayan rocks, the degassing effect will be prominent along the foothills of the MFT. Further, the Lesser and Higher Himalayan regions are highly rugged and hinder the consistent formation of anomalous belts/zones. Thermal infrared sensors like AVHRR on-board satellites like NOAA can record thermal changes up to 0.5°C during an overpass<sup>8</sup> which provides an important precursor before an impending earthquake<sup>6,8,9</sup>. This may be an important and novel way of analysing this complex natural phenomenon. In the night-time NOAA–AVHRR thermal images, a bright line indicating higher temperature

is observed at some places along the foothills of the Himalaya, which coincides with HFT and is termed as the ‘Himalayan thermal line’ (HTL). This has already been described<sup>6</sup> for the Chamoli earthquake that occurred on 29 March 1999 in Chamoli district, Uttarakhand, India. Similar occurrences of thermal anomalies prior to earthquakes have also been observed during the Bhuj earthquake<sup>9</sup> in Gujarat, India, which struck on 26 January 2001 at 23.39°N lat. and 70.31°E long. and the Algerian earthquake<sup>10</sup> which struck on 21 May 2003 at 36.97°N lat. and 3.85°E long.

Night-time scenes are better suited for any kind of land surface temperature (LST) study, especially for thermal anomaly in detecting subtle changes in thermal conditions compared to daytime scenes, which are marred by daytime differential solar heating effects<sup>11</sup>. Analysis of NOAA–AVHRR thermal images revealed that the HTL was only noticeable in night-time temperature images. Table 1 lists the night-time NOAA–AVHRR datasets acquired by the NOAA satellite earth station. Thermal channels 4 and 5 were used to generate LST time-series maps covering the 2015 Nepal earthquake-affected regions. An attempt was made to keep the time of acquisition of all scenes more or less consistent. The spatial resolution of NOAA–HRPT is 1.1 km with a temperature resolution of 0.5°C (ref. 11). A user-specified temperature range for the obtained scenes was considered in each case, which was taken as –30°C to +30°C for the night-time scenes. Scenes having cloud covers were identified and excluded for LST estimation. Image co-registration and correction for different satellite view angles were done to pinpoint the exact location of the observed HTL<sup>12</sup>.

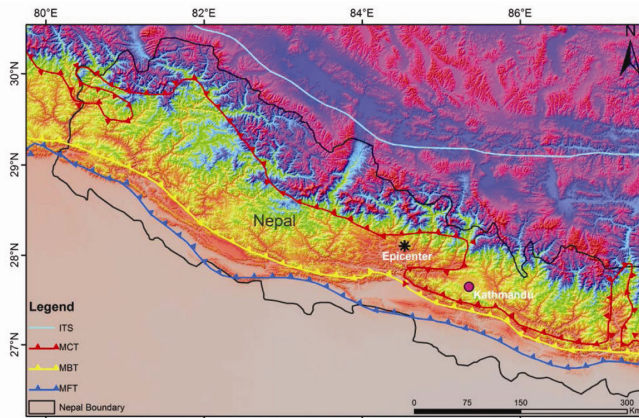


**Figure 1.** Shaded relief model showing the epicentre of the Nepal earthquake of 25 April 2015 and trends of the main thrust systems of the Himalaya. Tectonic features are from GSI<sup>3</sup>.

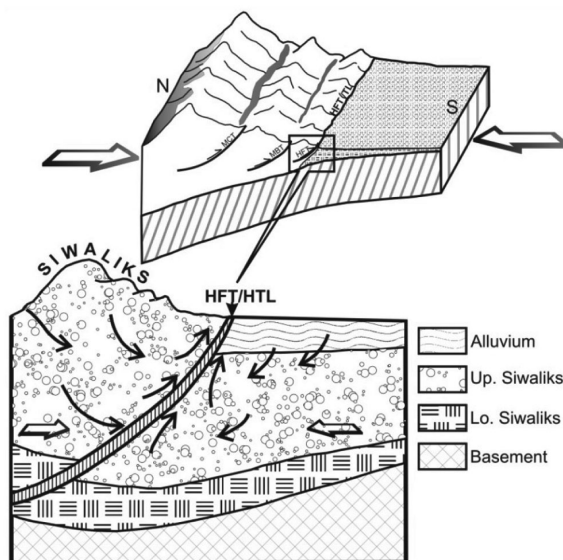


**Figure 2.** A schematic depiction of the ‘Himalayan thermal line’ along the foothills of the Himalaya<sup>6</sup>. Arrows show the movement of groundwater.

**Table 1.** Details of the NOAA–AVHRR digital thermal datasets used in the present study

Scene number	Date	Time of acquisition (IST, a.m.)
1	18 April 2015	02 : 58
2	19 April 2015	02 : 47
3	20 April 2015	02 : 36
4	21 April 2015	05 : 16
5	23 April 2015	02 : 01
6	24 April 2015	01 : 50
7	27 April 2015	02 : 58
8	29 April 2015	05 : 25

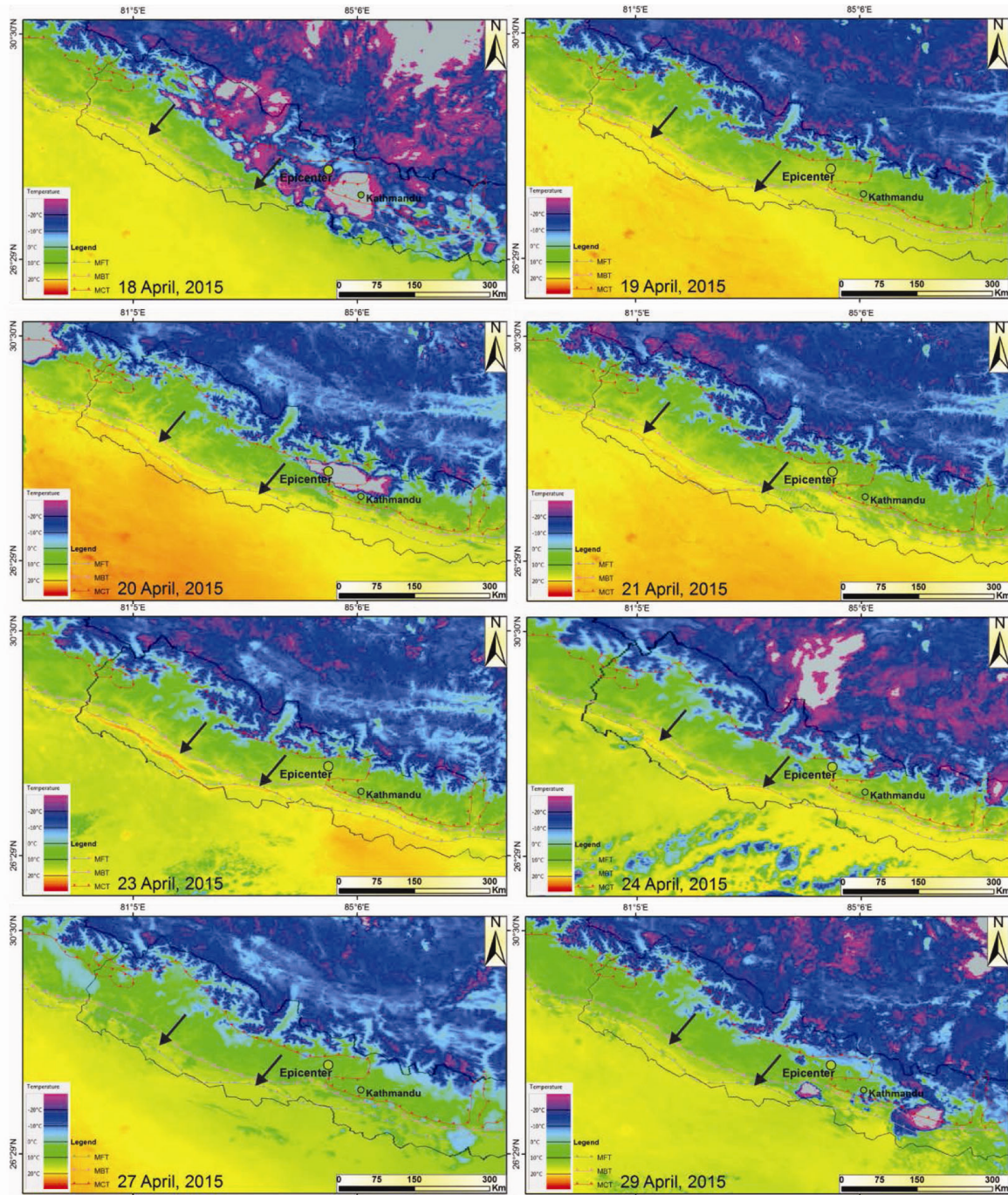


**Figure 3.** Night-time NOAA–AVHRR land surface temperature time-series map of Nepal before and after the earthquake on 25 April 2015.

Figure 3 shows a distinct anomaly in LST along the HTL, which appeared before the main earthquake event. This anomaly had appeared on 18 April 2015, around 150 km to the southwest of the epicentre, prior to the Nepal earthquake. The HTL reached its peak both in terms of intensity and extent along the MFT on 23 April 2015; it started dissipating one day before the earthquake and disap-

peared altogether with the main event. The temperature increase was about 7–8°C higher than the usual temperature of the region during this period. Time series night-time datasets of NOAA–AVHRR from 18 April 2015 to 29 April 2015 (i.e. six pre-earthquake datasets and two post-earthquake datasets) were used to infer the change in the extent of thermal anomaly along the HTL. Similar analysis

and processing of night-time NOAA–AVHRR data of the year 2014 acquired at around the same time and on the same days as the 2015 data, showed no such abnormal behaviour of the LST on those days in that year.

The AVHRR data of the NOAA series of satellites can be used to monitor an area on a regular and frequent basis. The thermal earthquake precursors can be used

to explain that earth degassing is behind the creation of a localized greenhouse effect. As this earthquake was caused by thrust faulting accompanying convergent tectonism, considerable emissions might have occurred along the foothills through the relatively porous and faulted media. From both the pre- and post-NOAA images, it can be deciphered that there are noticeable changes in the thermal regime along the MFT. On the NOAA thermal images, the thermal line is observed during the stress periods and disappears after the release of stress. Thus, it appears that changes in the thermal regime can be more extensively used to understand impending earthquakes.

1. Mitra, S., Paul, H., Kumar, A., Singh, S. K., Dey, S. and Powali, D., *Curr. Sci.*, 2015, **108**, 1938–1943.
2. United States Geological Survey, Nepal Earthquake Hazard Program: [http://earth-](http://earth-quake.usgs.gov/earthquakes/eventpage/us20002926#general_summary)

[quake.usgs.gov/earthquakes/eventpage/us20002926#general\\_summary](http://quake.usgs.gov/earthquakes/eventpage/us20002926#general_summary) (accessed on 15 May 2015).

3. GSI, *Seismotectonic Atlas of India and its Environs*, Geological Survey of India, 2000.
4. Valdiya, K. S., *Geology of the Kumaon Lesser Himalaya*, Wadia Institute of Himalayan Geology, Dehradun, 1980, p. 291.
5. Gansser, A., *Geology of the Himalayas*, Interscience Publishers, London, 1964, p. 273.
6. Saraf, A. K., Rawat, V., Tronin, A., Choudhury, S., Das, J. and Sharma, K., *J. Geol. Soc. India*, 2011, **77**, 195–204.
7. Qiang, Z. J. et al., *Sci. China*, 1999, **42**, 313–324.
8. Choudhury, S., Dasgupta, S., Saraf, A. K. and Panda, S., *Int. J. Remote Sensing*, 2006, **27**, 4381–4396.
9. Saraf, A. K. and Choudhury, S., *Int. J. Remote Sensing*, 2007, **26**, 1065–1073.
10. Saraf, A. K. and Choudhury, S., *Int. J. Remote Sensing*, 2005, **26**, 2705–2713.
11. Saraf, A. K. and Choudhury, S., *J. Indian Geophys. Union*, 2005, **9**, 197–207.

12. Tronin, A. A., *Int. J. Remote Sensing*, 2000, **21**, 3169–3177.

ACKNOWLEDGEMENT. We thank the Ministry of Earth Sciences, Govt of India for financial support.

Received 16 May 2015; revised accepted 17 September 2015

S. S. BARAL\*  
K. SHARMA  
A. K. SARAF  
J. DAS  
G. SINGH  
S. BORGHAIN  
E. KAR

Department of Earth Sciences,  
Indian Institute of Technology,  
Roorkee 247 667, India

\*For correspondence.  
e-mail: [suman.baral86@gmail.com](mailto:suman.baral86@gmail.com)

## Delineation of buried channels of Bharathappuzha by single-channel shallow seismic survey

Single-channel marine seismic surveys can identify the basic features of buried river channels. Since the methods deal basically with the subsurface acoustic reflectors, their termination, configuration, trend and dimension; any kind of incision changes the nature of the entire geometry. Palaeo channels are identified based on the analysis and interpretation of seismic data, according to the general concepts established in the field of seismic stratigraphy<sup>1,2</sup>. Generally, trunk/main channels have box-like, symmetric cross-sections, whereas smaller tributary channels have more V-shaped or asymmetric cross-sections<sup>3</sup>.

Bharathappuzha is the second longest river in Kerala, with a length of 209 km. The head waters of the main tributary of Bharathappuzha originate in the Anaimalai Hills, Western Ghats and flow westwards through Palakkad Gap and empty into the Arabian Sea at Ponnani. Biyyam Kayal is considered as the earlier mouth of Bharathappuzha, which enters into the Arabian Sea at Munambam, 8 km south of the present-day river mouth. Sea-level rise during the Holocene transgression has affected the

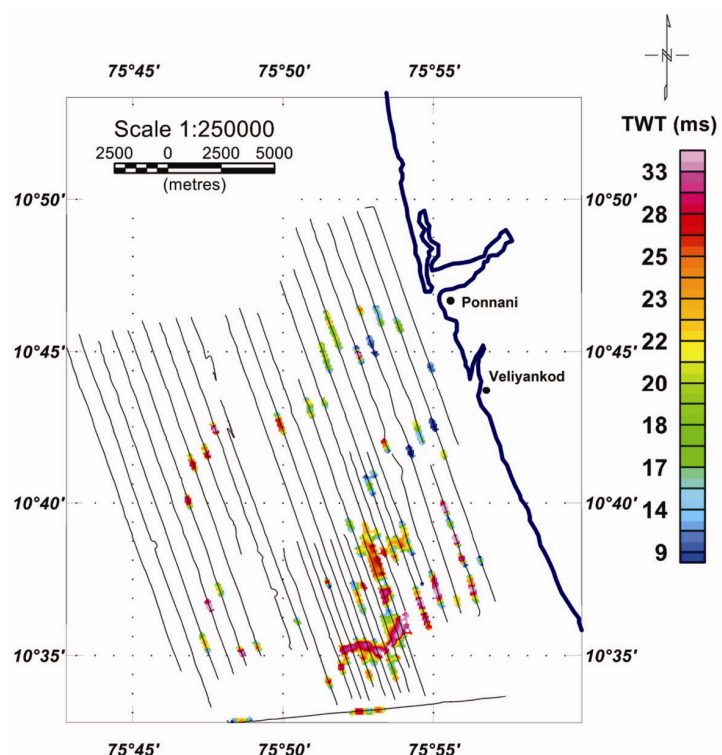


**Figure 1.** Two-way-travel (ms) of buried channel along with the cruise track off Bharathappuzha River, Kerala coast, India.